Defects in N, O and N, Zn implanted ZnO bulk crystals

Jan Eric Stehr, Xingjun Wang, Stanislav Filippov, S J. Pearton, Ivan Gueorguiev Ivanov, Weimin Chen and Irina Buyanova

Original Publication:

Jan Eric Stehr, Xingjun Wang, Stanislav Filippov, S J. Pearton, Ivan Gueorguiev Ivanov, Weimin Chen and Irina Buyanova, Defects in N, O and N, Zn implanted ZnO bulk crystals, 2013, Journal of Applied Physics, (113), 10.
http://dx.doi.org/10.1063/1.4795261

JOURNAL OF APPLIED PHYSICS **113**, 103509 (2013)

Defects in N, O and N, Zn implanted ZnO bulk crystals

J. E. Stehr,[1] X. J. Wang,[1,2] S. Filippov,[1] S. J. Pearton,[3] I. G. Ivanov,[1] W. M. Chen,[1] and I. A. Buyanova[1]
[1]*Department of Physics, Chemistry and Biology, Linköping University, 581 83 Linköping, Sweden*
[2]*National Laboratory for Infrared Physics, Shanghai Institute of Technical Physics, Chinese Academy of Sciences, 200083 Shanghai, China*
[3]*Department of Materials Science and Engineering, University of Florida, Gainesville, Florida 32611, USA*

(Received 15 January 2013; accepted 27 February 2013; published online 13 March 2013)

Comprehensive characterization of defects formed in bulk ZnO single crystals co-implanted with N and Zn as well as N and O atoms is performed by means of optically detected magnetic resonance (ODMR) complemented by Raman and photoluminescence (PL) spectroscopies. It is shown that in addition to intrinsic defects such as Zn vacancies and Zn interstitials, several N-related defects are formed in the implanted ZnO. The prevailed configuration of the defects is found to depend on the choices of the co-implants and also the chosen annealing ambient. Specifically, co-implantation with O leads to the formation of (i) defects responsible for local vibrational modes at 277, 511, and 581 cm^{-1}; (ii) a N-related acceptor with the binding energy of 160 ± 40 meV that is involved in the donor-acceptor pair emission at 3.23 eV; and (iii) a deep donor and a deep N_O acceptor revealed from ODMR. Activation of the latter defects is found to require post-implantation annealing in nitrogen ambient. None of these defects are detected when N is co-implanted with Zn. Under these conditions, the dominant N-induced defects include a deep center responsible for the 3.3128 eV PL line, as well as an acceptor center of unknown origin revealed by ODMR. Formation mechanisms of the studied defects and their role in carrier recombination are discussed. © *2013 American Institute of Physics*. [http://dx.doi.org/10.1063/1.4795261]

I. INTRODUCTION

ZnO is a wide band gap semiconductor that crystallizes in the wurtzite structure and has a direct band gap of ~3.3 eV at room temperature and a large exciton binding energy of 60 meV. Based on these properties, ZnO is currently considered as a promising candidate for applications in a wide variety of electronic and optoelectronic devices, such as UV light emitters and solar cells.[1–3] ZnO can also be used in gas sensors and may become a potential material for semiconductor spintronics as it exhibits room temperature ferromagnetism when appropriately doped.[4] In order to realize the full potential of ZnO in device applications it is necessary to control its electrical conductivity, i.e., to fabricate n-type and p-type conductive material. N-type doping in ZnO can be easily achieved via doping with Ga, Al, In, H, Cl, F, or I impurities that substitute their respective cation or anion host atoms and act as shallow donors. However, achieving reliable and reproducible p-type conductivity remains a great challenge since ZnO shows an asymmetry in dopability typical for the majority of wide band gap semiconductors.[5]

Nitrogen is considered as the most promising candidate as a p-type dopant in ZnO since it acts as a shallow acceptor in other II-VI compounds[6] and was also thought to be the most suitable anion-site acceptor in ZnO in view of both atomic-size and electronic-structure considerations.[7] Several groups have indeed reported successful p-type doping of ZnO with nitrogen,[8–12] yet such p-type conductivity often degraded in a period of several days.[11] Also, although N incorporation has been found to cause formation of a relatively shallow acceptor with a binding energy of around 170 meV, based on the observation of the related donor-acceptor-pair (DAP) emission,[13–15] the doped materials often remained semi-insulating or n-type conducting. Now the question arises why no reliable p-type doping can be achieved even when a high amount of N is provided during growth. Several effects can, in principle, contribute to this problem. First of all, N incorporation may be affected by polarity of ZnO as pointed out by Lautenschläger *et al.*[16] Second, even when N is incorporated in ZnO its efficiency as an acceptor is expected to largely depend on local surrounding and the presence of other impurities. For example, nitrogen substituting for oxygen, N_O, is a deep acceptor[17–20] with an energy level of $E_v + (1.6–1.7)$ eV.[20] On the other hand, the acceptor ionization energy is predicted to be significantly reduced if (i) N_O is surrounded by isovalent group II atoms substituting Zn (Ref. 17); (ii) N_O is a part of complexes with residual group III contaminants (Al, Ga, In);[21] or (iii) N_O forms the N_O–H–N_O complex.[22] Moreover, the electrical activity of N can be largely affected by the presence of various intrinsic defects which can act as efficient compensating centers[23,24] and also facilitate formation of various N-related complexes.

In order to address the last issue it is essential to simultaneously control N incorporation and defect formation in ZnO. This can be achieved by using, e.g., ion implantation as this technique not only provides the possibility to incorporate a controllable amount of dopants (by choosing an implantation dose) but also to maximize formation of certain intrinsic defects (by co-implantation with O or Zn). It is also critical to employ characterization techniques capable of providing information on the origin of the formed defects.

A powerful tool to investigate chemical identity and local structural properties of defects in semiconductors is magnetic resonance (MR) spectroscopy. In ZnO, this technique has provided MR signatures and, in certain cases, also energy level positions of common intrinsic defects, such as zinc and oxygen vacancies, zinc interstitials (Zn_i), and common residual contaminants including Li, Na, H, Al, Ga, etc. (see, e.g., Ref. 25 for an overview). Traditional MR methods such as electron paramagnetic resonance (EPR), however, face several difficulties when defect characterization should be performed only within a limited volume of the structure such as an implanted region. The most severe problem is that EPR is a volume-sensitive method that will probe all defects present in the structure. Even in the case when the defects solely exist within the implanted region, the low total number of defects could fall below the EPR detection limit if the implanted volume is small. This problem can be overcome by the optically detected magnetic resonance (ODMR) technique, as it combines chemical sensitivity of magnetic resonance with high sensitivity of optical method. Moreover, ODMR signals can be detected via light emissions specific for the region of interest providing information on its defect properties, as has been recently demonstrated for ZnO epilayers,[26,27] as well as P-implanted ZnO.[28] In this work we employ this technique complemented by photoluminescence (PL) and Raman measurements to perform comprehensive characterizations of defects formed in bulk ZnO single crystals co-implanted with N and Zn as well as N and O atoms.

II. EXPERIMENTAL DETAILS

We have investigated the (0001)-oriented nominally undoped ZnO bulk single crystals from Cermet Inc. One of the samples was left untreated for a comparison. The other samples were co-implanted at 300 K either with N^+ and Zn^+ (to be referred to as ZnO:(N,Zn)) or with N^+ and O^+ ions (to be referred to as ZnO:(N,O)). Ion implantation was performed in a non-channeling direction. In order to create approximately uniform profiles of the implanted nitrogen atoms with a concentration of around $2 \times 10^{18}\,cm^{-3}$, ion energies of 30 keV (dose of $6 \times 10^{12}\,cm^{-2}$), 60 keV (dose of $1.2 \times 10^{13}\,cm^{-2}$), 120 keV (dose of $2.5 \times 10^{13}\,cm^{-2}$), and 200 keV (dose of $5 \times 10^{13}\,cm^{-2}$) were used. The distribution of the implanted nitrogen atoms calculated by using the stopping and range of ions in matter (SRIM) code is shown in Figure 1. Doses and energies for the zinc and oxygen co-implantations were chosen in a way to overlap with the distribution of the nitrogen atoms. The total thickness of the implanted layers was about 500 nm. After implantation the samples were annealed by rapid thermal annealing (RTA) at 800 °C for 2 min under a flowing O_2 or N_2 ambient. In previous experiments this annealing temperature has been found to provide optimal conditions for removing implantation damage while avoiding preferential loss of oxygen from the ZnO surface.[14,28] During annealing, the implanted samples were placed face down on sacrificial ZnO crystals in order to minimize surface degradation.

Raman measurements were carried out with a Horiba LabRam HR 800 spectrometer at room temperature (RT) using the 532 nm line of a Nd:YAG laser as an excitation source. Photoluminescence was excited by using the 351 nm line of an Ar^+ ion laser. The PL signals were spectrally dispersed by a grating monochromator and detected at 5 K by a charge-coupled-device (CCD) camera or a germanium detector, depending on monitored spectral ranges. ODMR measurements were performed at 3 K with a microwave (MW) frequency of 9.21 GHz (X-band) and a MW power adjustable between 1 and 200 mW. The ODMR signals were measured as MW-induced changes of the PL intensity by a Si detector in the visible region and were detected by a Ge detector in the near-infrared region. Spectral dependences of the ODMR signals were obtained by selecting desired spectral windows for the PL detection with the aid of appropriate optical filters. Angular dependent ODMR measurements were performed by varying an angle θ between the direction of an applied magnetic field **B** and the direction of the crystallographic c-axis of the ZnO crystals.

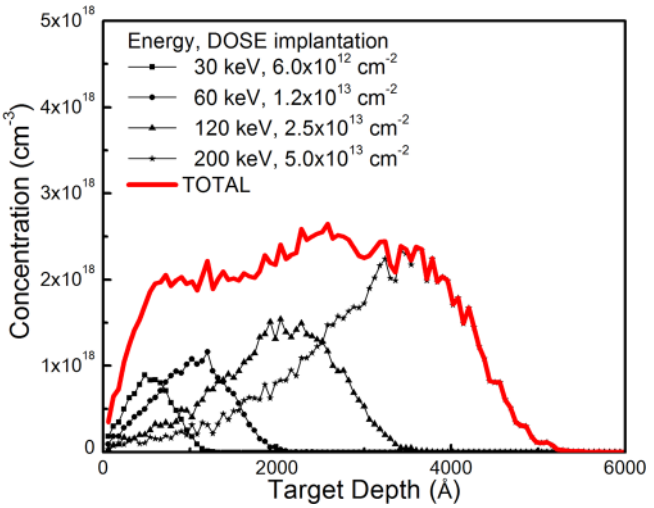

FIG. 1. Distribution of the implanted nitrogen atoms calculated by using the stopping and range of ions in matter (SRIM) code.

III. RESULTS AND DISCUSSION

A. Raman spectroscopy

Figure 2 shows Raman spectra of the investigated untreated and implanted samples obtained under the 532 nm excitation. The spectra are dominated by the well-known non-polar E_2^{low} and E_2^{high} modes centered at 99 cm^{-1} and 438 cm^{-1}, respectively, as well as the modes $2E_2^{low}$ (205 cm^{-1}) and E_2^{high}-E_2^{low} (333 cm^{-1}). These modes are present in all samples and are characteristic for wurtzite ZnO. The samples co-implanted with N and O show three additional Raman modes at 277 cm^{-1}, 511 cm^{-1}, and 581 cm^{-1}, which are labeled in Fig. 2 as LVM1, LVM2, and LVM3, respectively. The same modes have been reported earlier in the literature, and several controversial models have been proposed. Kaschner *et al.* observed them in N-doped thin films grown by chemical vapor deposition (CVD) and attributed them to local-vibrational-modes (LVMs) related to nitrogen motion.[29] This model was also consistent with results of Reuss *et al.* who observed appearance of the

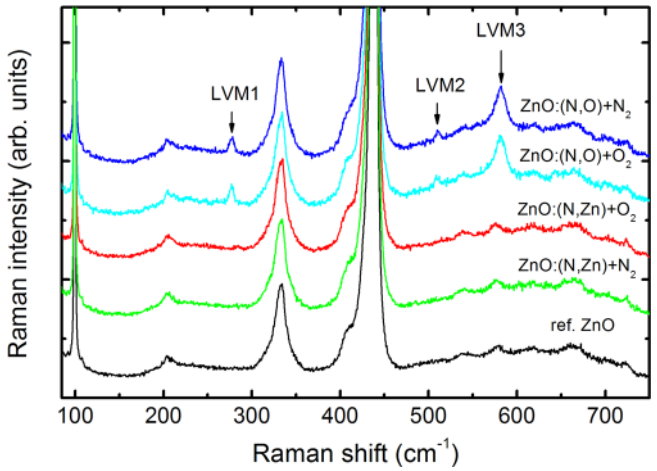

FIG. 2. Raman spectra measured at RT from the ion-implanted and reference ZnO samples.

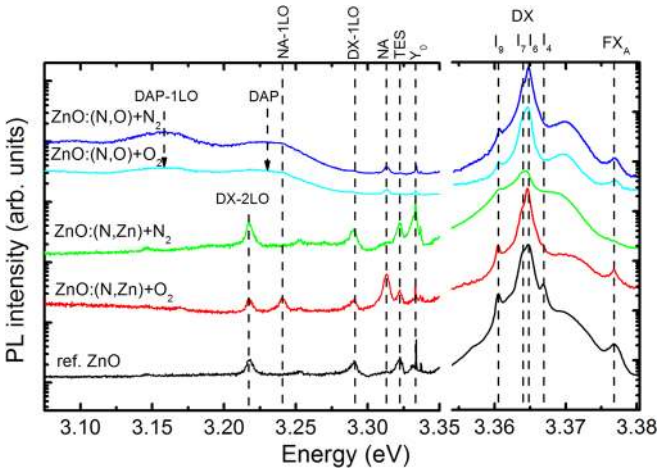

FIG. 3. PL spectra measured at 5 K within the NBE region from the ion-implanted and reference ZnO samples. The spectra are shown in the semi-logarithmic scale and are offset vertically for clarity. The PL intensities are about 600 times weaker in the implanted structures.

same modes in N^+-implanted ZnO.[14] Alarcon-Lado *et al.*,[30] however, pointed out that although the modes are indeed related to the presence of N, they do not involve N motion as their frequencies do not change for different N isotopes. Friedrich *et al.*[31] have also confirmed that the modes are activated by the N presence but established that the LVM1 and LVM2 modes involve vibrations of Zn atoms, based on the observed influence of Zn isotopes on the LVM frequencies. They have suggested that the presence of nitrogen in the ZnO lattice induces a local lattice distortion that favors the formation of Zn_i-related defect complexes (Zn_i-N_O) (275 cm^{-1}) and (Zn_i-O_i) (510 cm^{-1}). The suggested model was supported by the *ab initio* density functional calculations as well as by calculations of Wang *et al.*[32]

Our results are consistent with the idea that the formation of defects responsible for LVM1-LVM3 modes is facilitated by the N presence. However, they also clearly demonstrate that the defect formation critically depends on overall defect environment that is modified by the presence of co-implanted atoms. Surprisingly, the LVM modes were not detected after co-implantation with zinc (see Fig. 2), i.e., under favorable conditions for the formation of Zn_i as confirmed from the performed ODMR measurements (to be discussed below). On the other hand, the presence of excess oxygen seems to play a crucial role implying that either the defect formation is enhanced by O implantation or the O atom is a part of the defect complex(es) responsible for the LVM1-LVM3 modes. Further studies on O isotopes-enriched ZnO are required to clarify this issue.

B. Photoluminescence

Figure 3 presents an overview of PL spectra measured within the near-band-edge (NBE) spectral region before and after the ion implantation. The PL spectrum of the untreated sample is typical for undoped ZnO and contains I_4, I_6, I_7, and I_9 lines due to recombination of donor bound excitons (DX),[33] as well as free exciton (FX) emission. On the low energy side of the spectrum, two electron satellite (TES) transitions of the DXs are observed. These PL transitions are followed by their longitudinal optical (LO) phonon replica labeled as DX-1LO, DX-2LO, and TES-1LO. At 3.333 eV one can also observe the Y_0 line, which was assigned to excitons bound to extended structural defects by Wagner *et al.*[34]

Ion implantation and subsequent annealing (to be referred to as treatment) have several effects on the NBE PL spectra. First of all, intensities of all aforementioned emissions are substantially (by about 600 time) quenched after the treatment which can be attributed to formation of defects that act as competing recombination centers. One also notices that the I_4 line can no longer be detected in the treated samples. Even though this could be due to annealing-induced out-diffusion of hydrogen, which is known to be stable in ZnO only under thermal annealing at temperatures below 500 °C,[33,35–37] we have not observed the complete quenching of this emission in the P-implanted samples annealed under the same conditions.[28] This may indicate that in the N-implanted ZnO hydrogen is partly consumed by forming complexes with N atoms.[22,38,39]

Second, the PL spectra of the treated samples contain additional sharp PL lines at 3.3128 and 3.2405 eV labeled as NA and NA-LO in Fig. 3. These lines have been previously observed[8,12,40,41] in N-doped ZnO and were attributed to no-phonon and LO-assisted radiative transitions which involve a deep N acceptor. The exact origin of the responsible recombination process remains, however, highly controversial as the emission has been assigned to recombination of excitons bound to a neutral acceptor (A^0X)[8,42] and also to free electron to acceptor (FA) transitions.[43] The former model seems to be more likely, judging from a relatively narrow (~5 meV) line width of the NA line. Assuming that the Hayne's rule is applicable to A^0X transitions, Look *et al.*[8] have placed an energy level of the involved acceptor as being E_v + 240 meV. This value is too small to be related to the substitutional N_O acceptor. Therefore, the involved defect is most likely a complex that contains an N atom. From Fig. 3, the intensity of the NA lines is the highest in the ZnO co-implanted with N and Zn and annealed in oxygen ambient (denoted as ZnO:(N,Zn)+O_2) but is the lowest when the annealing is performed in nitrogen ambient

(denoted as ZnO:(N,Zn)+N_2). This may suggest that the defect formation is favored under Zn-rich conditions but is suppressed by oxygen deficiency.

The samples co-implanted with N and O exhibit an additional broad PL band which is centered at around 3.23 eV and is accompanied by LO-assisted transitions. This emission was observed earlier by several groups and was assigned to DAP transitions related to a nitrogen acceptor.[9,13,14,44] The acceptor ionization energy was estimated as being 160 ± 40 meV (Ref. 9) under the assumption that the donor participating in the DAP transitions is a shallow donor with the ionization energy of 52 meV. This value again indicates that the involved N-related acceptor is likely a complex defect. From Fig. 3 the defect formation is enhanced in the O-rich environment. The presented results of PL measurements clearly show that several N-related acceptors can be formed in ZnO, and their local configuration largely depends on other defects present in the material.

In addition to changes in the NBE emission, N implantation and subsequent annealing also cause modifications of the PL spectra within the visible and near-infrared spectral ranges as shown in Figures 4(a) and 4(b), respectively. In the case of the untreated sample, the PL spectrum contains a broad PL band ranging from 1.6 to 2.5 eV that consists of several overlapping emissions with peak positions at around 1.75, 1.95, 2.15, and 2.4 eV. After implantation and subsequent annealing the PL band centered at 2.4 eV is quenched in all cases whereas the intensities of other PL bands depend strongly on the conditions of the treatments. For example the PL band peaking around 1.75 eV is present in all implanted samples but is more intense in the samples annealed in O_2 ambient which was also observed in Refs. 28 and 45 for P implanted ZnO. The emissions with energies higher than 2.1 eV are suppressed in the samples co-implanted with O, ZnO:(N,O). This is not surprising since these PL bands are often associated with defects related to oxygen deficiency that can be reduced by co-implantation with oxygen. From Fig. 4(b), co-implantation with N and O also leads to the appearance of a broad infrared PL band centered at 1.17 eV. The observed changes in the PL spectra imply significant modifications in the defect properties of the investigated samples upon implantation and annealing.

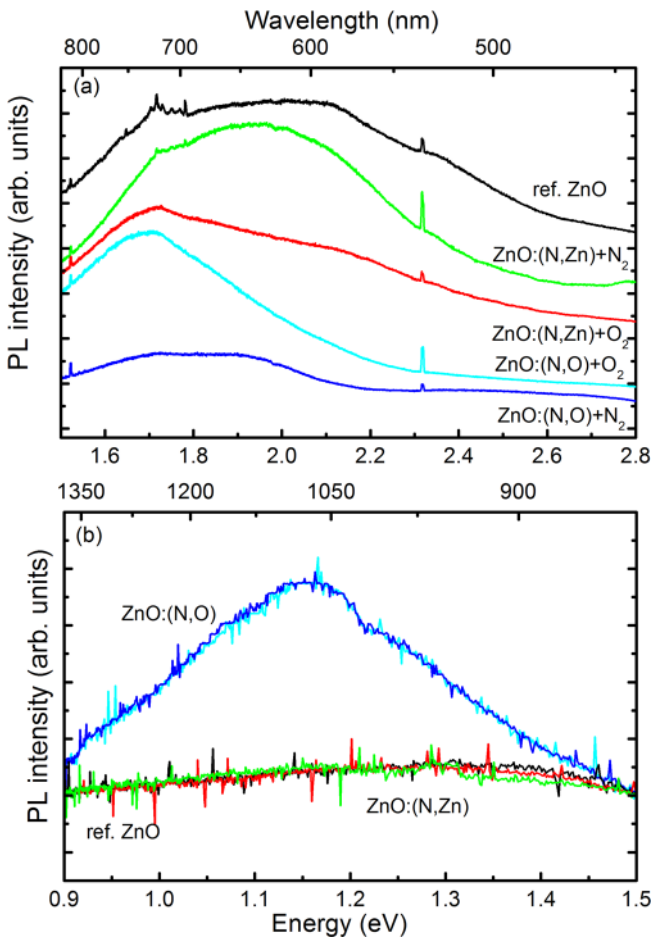

FIG. 4. RT PL spectra measured from the studied structures within the visible (a) and near-IR (b) spectral ranges. The spectra are shown in the semi-logarithmic scale.

C. ODMR

1. Defect signatures

To further understand the effects of N and O as well as N and Zn implantation on the defect formation in ZnO we have conducted ODMR measurements. With this technique it is possible to trace various paramagnetic defects that are active in recombination processes since each defect in most cases possesses a unique set of Spin-Hamiltonian parameters, which could be used for its identification. In order to analyze the ODMR results the data were fitted with the help of Easyspin using the following Spin-Hamiltonian:[46]

$$\mathcal{H} = \mu_B \boldsymbol{BgS} + \boldsymbol{SAI} + \boldsymbol{IQI} - g_N \mu_N \boldsymbol{BI}. \quad (1)$$

Here the first term denotes the electronic Zeeman energy, μ_B denotes the Bohr magneton, **B** the external magnetic field, **S** the electron spin, and **g** the electron g-tensor. The second term describes the hyperfine interaction involving nuclear spin I, quantified by the hyperfine tensor **A**. The third term accounts for a quadrupole interaction **Q** arising for nuclei with spin $I > 1/2$ from the interaction with an electric field gradient at the site of the nucleus. The last term in Eq. (1) is the nuclear Zeeman energy. The spin-Hamiltonian parameters of all ODMR signals discussed below are summarized in Table I. The defect formation was found to substantially depend on conditions of the treatment as will be discussed in detail hereafter.

a. Co-implantation with nitrogen and oxygen, ZnO:(N,O). Figure 5 shows representative ODMR spectra from the ZnO:(N,O) samples together with a spectrum of the untreated reference ZnO crystal. All spectra were obtained by monitoring the defect related broad PL bands in the visible spectral range (see Fig. 4(a)) as intensities of the N-induced emissions within the NBE spectral range were too low to allow ODMR measurements. The ODMR spectrum of the reference crystal is depicted by the lowest curve in Fig. 5 and contains several signals which can be identified based on the determined spin-Hamiltonian parameters. The signal located on the high-field side of the spectrum can be ascribed

TABLE I. Summary of the spin-Hamiltonian parameters of the defects revealed by ODMR in this work. For the non-axial centers, φ is the angle between the z and $\boldsymbol{c}$ axis. $A_\perp$, $A_\parallel$, and e^2qQ/h are given in MHz.

		Axial		Nonaxial							
Center	S	$g_\perp$	$g_\parallel$	g_{xx}	g_{yy}	g_{zz}	$A_\perp$	$A_\parallel$	e^2qQ/h	η	φ (deg)
V_{Zn}^-	1/2	2.0213	2.0061	2.0203	2.0227	2.0061					110.75
V_{Zn}/Zn_i	1			1.9888	1.9893	1.9815					110.75
V_{Zn}/EM	1			1.9862	1.9866	1.9799					110.75
Zn_i^+	1/2	1.9595	1.9605								0
EM	1/2	1.955	1.957								0
D2	1/2	1.977	1.973								0
N_O	1/2	1.963	1.995				8.5	81.1	−5.9	0.05	0

to an effective-mass (EM) donor with $g \approx 1.96$. The two signals on the low-field side originate from the non-axial and axial configurations of the negatively charged zinc vacancy (V_{Zn}^-), denoted in Fig. 5 as $V^-_{Zn(na)}$ and $V^-_{Zn(a)}$, respectively. The signal related to a pair defect of the EM donor and V_{Zn}^- acceptor (V_{Zn}/EM) with $S = 1$ is seen in the center of the spectrum.[47] Such spin-triplet systems which consist of an exchange coupled pair of a donor (D) and an acceptor (A) are quite common in ZnO (Refs. 28, 47, and 48), and the corresponding g-value can be estimated by $g \sim [g(D) + g(A)]/2$. In previous works it was shown that these centers often contain relatively distant D-A pairs as the related ODMR signals could be suppressed at high MW modulation frequencies due to a slow recombination rate of these distant pairs.[47] This is, however, not the case for the V_{Zn}/EM spin triplet center observed here since intensity of the central peak was not quenched even at MW modulation frequencies of about 10 kHz. This leads to the suggestion that the partners of the complex are located in close proximity to each other. All these signals can also be detected via the near-IR emission, consistent with earlier studies.[28]

The same V_{Zn}^-, V_{Zn}/EM, and EM defects are also formed in ZnO:(N,O)+O_2 (see Fig. 5). This is probably not surprising since zinc vacancies are among the primary intrinsic defects that can be created by ion bombardment. Moreover, they exhibit the highest thermal stability among all intrinsic defects[48] and are also favored from thermodynamics considerations under oxygen-rich conditions. This should be the case when the excess oxygen was incorporated via co-implantation, and post-implantation annealing was performed in oxygen ambient.

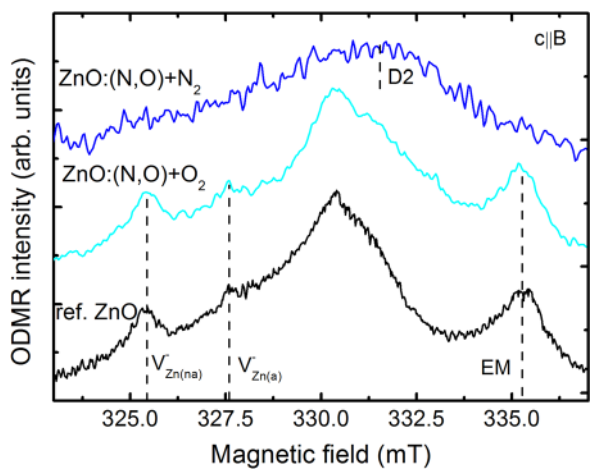

FIG. 5. Representative ODMR spectra measured at 3 K and 9.214 GHz from ZnO:(N,O) after annealing in N or O ambient. For comparison, also shown is the ODMR spectrum from the untreated reference ZnO. The spectra were obtained by detecting the defect-related emissions within the visible spectral range shown in Fig. 4(a).

The situation, however, changes drastically when co-implantation with N and O was followed by annealing in N_2 ambient. None of the aforementioned signals are any longer pronounced in the spectra. They are replaced by a broad ODMR signal that is centered at around 331.4 mT. An angular dependence of this signal, which is labeled as D2 in Fig. 5, is shown in Figure 6. It can be best simulated assuming an axial center with $S = 1/2$ and the electron g-values of $g_\parallel = 1.973$ and $g_\perp = 1.977$. The simulated angular dependence of D2 as well as the traces of the EM donor are indicated in Fig. 6 by the vertical lines. Judging from the deduced g-values, the D2 signal is most likely related to a deep donor. A possible candidate is an N_{Zn} donor that is favorably formed under O-rich conditions.[49] The formation of this defect can then also explain the observed reduction of the V_{Zn}^- signal.

The D2 signal can also be detected by monitoring the near-IR emission (see Figure 7) where the corresponding ODMR spectra of ZnO:(N,O)+N_2 are shown. In this spectral range, however, an additional signal labeled as N_O in Fig. 7 is observed. In order to study the origin of the corresponding defect in more detail we performed ODMR measurements for several orientations of a static applied magnetic field **B** relative to the c-axis (see Figures 7(a)–7(c)) for θ equals to 90°, 70°, and 40°, respectively. It is found that the N_O signal is strongly anisotropic, and its angular behavior can be simulated assuming that it is related to a nitrogen acceptor substituting oxygen (N_O).[20,50] In Fig. 7, the simulations of the complete spectra, which were performed assuming involvement of N_O and D2, are depicted by the solid lines whereas the dashed lines show individual contributions of the N_O and D2 signals. A good agreement between the simulated and experimental spectra is observed, which confirms the suggested assignment of the signals.

b. Co-implantation with nitrogen and zinc, ZnO:(N,Zn). Figure 8 depicts representative ODMR spectra

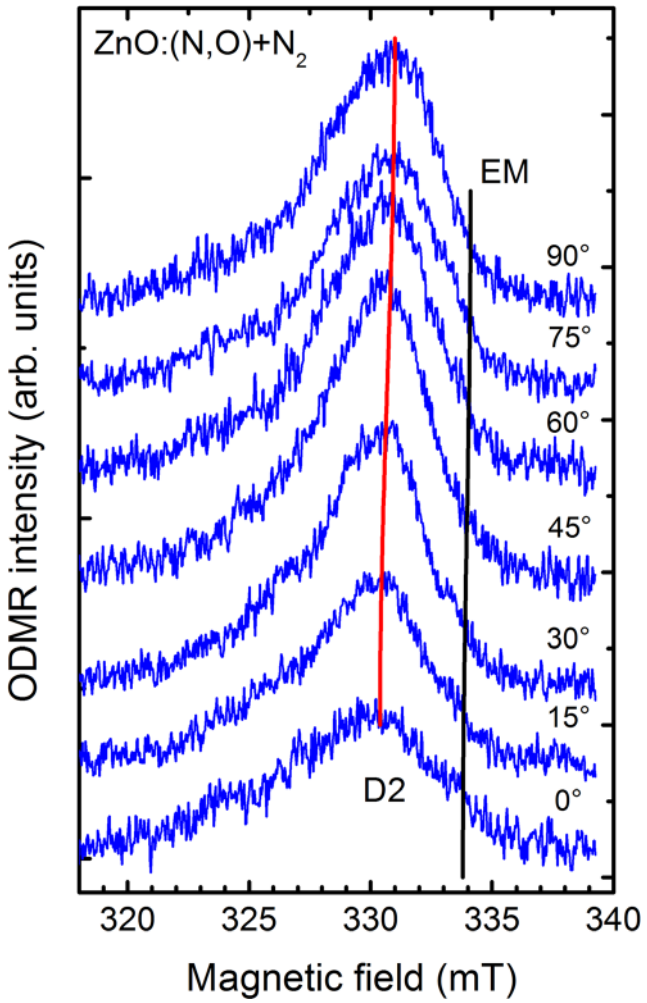

FIG. 6. Angular dependent ODMR spectra measured at 9.144 GHz from ZnO:(N,O)+N_2 by monitoring the defect-related PL emission within the visible spectral range shown in Fig. 4(a). The vertical lines indicate the angular dependences of D2 and the EM donor.

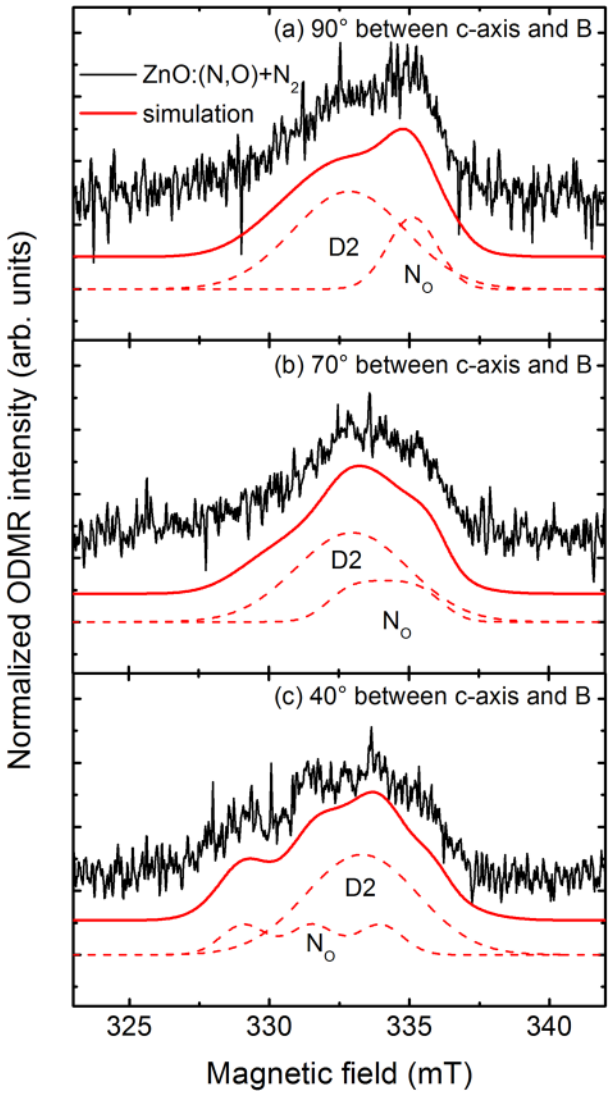

FIG. 7. ODMR spectra measured at 9.214 GHz from ZnO:(N,O)+N_2 by monitoring the defect-related PL emission within the near-IR spectral range, shown by the top curves (black online) in (a)-(c). The spectra were measured for the following angles θ between the direction of a static applied magnetic field **B** and the orientation of the c-axis: (a) $\theta = 90°$, (b) $\theta = 70°$, and (c) $\theta = 40°$. The thick solid curves (red online) are ODMR spectra simulated with the aid of the Spin-Hamiltonian (Eq. (1)) including contributions from the D2 and N_O signals. The simulated spectra for each defect are shown by the dashed curves (red online).

from the ZnO:(N,Zn) samples measured under different orientations of an applied static magnetic field **B** relative to the c-axis. All spectra were obtained by monitoring the defect-related broad PL bands in the visible spectral range (see Fig. 4(a)). The spectra measured from ZnO:(N,Zn)+O_2 and ZnO:(N,Zn)+N_2 are shown by the solid lines (red online) and dots (green online), respectively. The latter is only shown for **B**||**c** as the detected signals have similar angular dependences in both materials but are stronger in ZnO:(N,Zn)+O_2. A careful analysis of the measured angular dependences by using the spin-Hamiltonian (Eq. (1)) reveals that the measured spectra contain contributions from several defects as will be specified below. At the low-field side of the spectra, V_{Zn} still dominates but is no longer the only acceptor-type defect. This is more apparent from Figure 9 where field positions of the corresponding signals are summarized. Additional ODMR signals, depicted by open symbols (red online) in Fig. 9, can be clearly resolved when the direction of B is turned off the c-axis. Unfortunately, determination of the corresponding spin-Hamiltonian parameters is hampered by week intensities and a strong overlap of these signals with V_{Zn}^-. Judging from their field positions, these additional signals originate from a non-axial center acting as an acceptor. Most likely, it is related to a complex defect that involves N (and possibly Zn) as this paramagnetic center was so far not reported in ZnO.

Furthermore, the EM donor can no longer alone explain the shallow donor signals around $g = 1.96$ as shown in Fig. 8. The second signal that is seen as a low-field shoulder of the EM signal can be assigned to zinc interstitials (Zn_i). The formation of Zn_i can be understood as a result of the co-implantation with zinc that leads to a high amount of off-stoichiometric zinc in the sample. Due to the change in the acceptor type defects, the exchange-coupled defects of V_{Zn} and EM or Zn_i cannot fully account for the broad ODMR signal around $g = 1.98$ as the change of the acceptor g-value affects the g-value of the related pair defects.

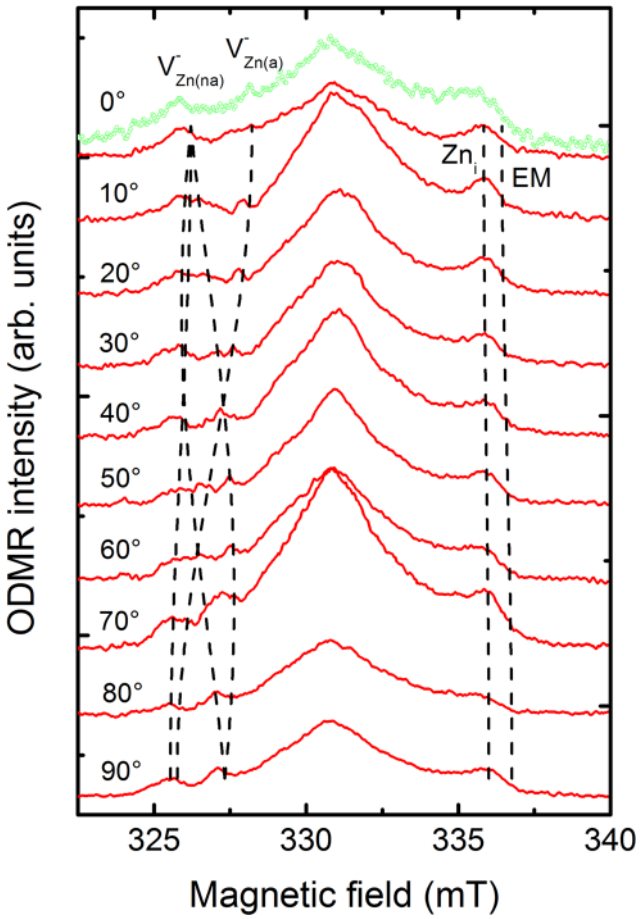

FIG. 8. Representative ODMR spectra measured at 3 K and 9.214 GHz from ZnO:(N,Zn)+O_2 (solid lines, red online) and ZnO:(N,Zn)+N_2 (open circles, green online) by monitoring the defect-related PL emission within the visible spectral range shown in Fig. 4(a). The spectra are measured under different orientations of the magnetic field B relative to the crystallographic c-axis as stated in the figure. The sample was rotated in the (1100) plane. The dashed lines indicate angular dependences of the V_{Zn}, Zn_i, and EM signals.

2. Role of the defects in radiative recombination

All detected ODMR signals have a positive sign, which means that intensities of the monitored PL emissions are enhanced as a result of microwave induced transitions between spin-split sublevels of the defect centers. This often indicates direct involvement of the defect in the monitored recombination process and, therefore, allows one to single out PL emissions related to specific defects based on spectral dependences of the ODMR signals. Previous studies of electron-irradiated,[47,51] as-grown[48,52,53] as well as P-implanted ZnO (Ref. 28) have unambiguously established that the V_{Zn}^- and EM defects participate in the spin-dependent radiative recombination process associated with the "red" PL band, which is centered at around 1.6 eV and has a zero phonon line at 2.4 eV. The same conclusion is also valid for the studied ZnO:(N,Zn) and ZnO:(N,O)+O_2.

The N_O signal, on the other hand, is detected via the IR emission with photon energies below 1.5 eV although a detailed spectral dependence of this signal cannot be measured in this study, unfortunately, due to a very low signal intensity. The N_O center is known to be a deep acceptor with an energy level position of E_v + 1.6 eV (Refs. 19, 20, and 54). The spin-dependent process that is observed by ODMR is likely the capture of an electron by N_O^0, i.e.,

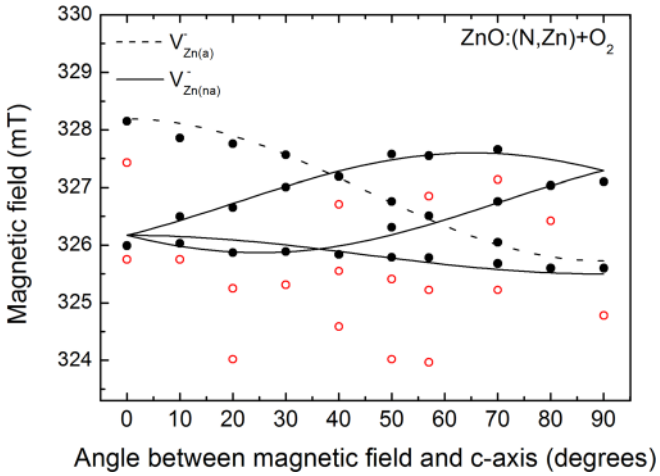

FIG. 9. Angular dependences of the ODMR signals measured at 9.214 GHz from ZnO:(N,Zn)+O_2. The sample was rotated in the (1100) plane. The symbols denote the experimental points, and the lines are simulations from Eq. (1) using the spin-Hamiltonian parameters given in Table I. The open symbols (red online) are field positions of the N-induced ODMR signal from a N-related non-axial center acting as an acceptor.

$$e^- + N_O^0 \rightarrow N_O^- \tag{2}$$

or

$$D2^0 + N_O^0 \rightarrow D2^+ + N_O^-, \tag{3}$$

if the D2 donor is also involved. The PL process can then be attributed to the capture of a hole by N_O^-, which together with the spin-dependent process (2) or (3) completes an excitation-recombination cycle. We note, though, that this PL process is not responsible for the 1.17 eV PL band detected in ZnO:(N,O) (see Fig. 4(b)). This is because this PL band is observed in both ZnO:(N,O)+O_2 and ZnO:(N,O)+N_2 samples whereas the N_O ODMR signal is only detected in ZnO:(N,O)+N_2.

IV. SUMMARY

The presented results clearly show that a number of N-related defects can be formed in ZnO and that the prevailed defect configuration may be altered by co-implantation and also by a choice of annealing ambient. Specifically, co-implantation with oxygen leads to the formation of several N-related defects that can be detected by the Raman, PL and, ODMR techniques:

(i) From the Raman measurements, it is found that the presence of N leads to the appearance of three local vibrational modes at 277 cm^{-1}, 511 cm^{-1}, and 581 cm^{-1}. Although this effect is well documented in the literature,[14,29–31] the present work shows that the formation of the involved defects is largely enhanced by co-implantation with O (see Fig. 2). Such behavior is consistent with the suggested origin of the 511 cm^{-1} mode as being due to the (Zn_i-O_i) complex.[31] However,

it may be unexpected for the 277 cm^{-1} mode as it was assigned by Friedrich *et al.*[31] to the Zn_i-N_O complex.

(ii) From PL, co-implantation with N and O provides favorable conditions for the formation of a N-related acceptor with the binding energy of 160 ± 40 meV that is responsible for the DAP emission at 3.23 eV (Fig. 3(a)). This binding energy is very close to the calculated energy level of the N_{Zn}-$2V_{Zn}$ complex,[49] which is expected to be formed under Zn-deficiency.

(iii) From ODMR, such treatment causes the formation of a new deep donor (labeled as D2) and a deep N_O acceptor (with the energy level of $E_v + 1.6$ eV) that participates in the near-IR emission. We note that activation of these defects requires the post-implantation annealing in N_2 ambient (see Figs. 4–6).

None of these defects are detected, however, when co-implantation is performed with Zn instead of O. Here, the dominant N-induced defects include a deep center responsible for the 3.3128 eV PL line (denoted as NA in Fig. 3(a)), as well as an acceptor center of unknown origin detected via ODMR (see Figs. 8 and 9). Both defects are present in higher concentrations after post-implantation annealing in O_2 ambient.

At the first glance, some of the aforementioned findings seem to be rather surprising and even puzzling as they imply that the formation of acceptors that were previously attributed to N_O (or related complexes) can be facilitated by co-implantation with oxygen. This is in spite of the fact that such co-implantation creates the oxygen-rich environment and that O and N atoms compete for the same lattice sites. Moreover, formation energies of N-related acceptors (both isolated N_O a as well as related complexes) are theoretically predicted[19,49] to be lower in n-type ZnO. Therefore one expects that co-doping with shallow donors should facilitate the N-incorporation. Such conditions are more likely in Zn-rich ZnO as Zn_i and V_O, which have low formation energies under these conditions, behave as shallow donors.

Assuming that the previous assignments are correct, a possible explanation for this unexpected behavior could be as follows. First of all, the defect formation energies have been calculated based on thermodynamic considerations which may not be fully applicable when doping is accomplished via ion implantation. Instead, one may also consider probabilities of bombardment-induced kick-off processes in O and Zn sub-lattices by light and heavy atoms, such as O and Zn, respectively. The maximum energy which can be transferred during the head-on collision from a moving ion to a lattice atom depends on their mass difference. Therefore, the maximum energy which can be transferred from an impinging O^+ ion to a O lattice atom is about 6 time higher than that to a Zn lattice atom whereas the reverse is true for a Zn^+ ion. Although the Rutherford cross-section is larger for heavier atoms, one may still expect relatively higher damage in the oxygen sublattice under co-implantation with O^+. This would create oxygen vacancies (V_O) and, therefore, provide favorable conditions for the formation of N_O and related complexes if probability of trapping of nitrogen by V_O is at least comparable to that for O. Such process should be further facilitated when the access oxygen atoms supplied via implantation out-diffuse from the crystal, e.g., under annealing in nitrogen ambient, consistent with our ODMR data for ZnO:(N,O)+N_2. If the proposed scenario is true, co-implantation with light or heavy atoms may provide a useful approach to facilitate formation of N acceptors in configurations that are desirable for inducing p-type conduction of the material.

ACKNOWLEDGMENTS

Financial support by the Swedish Research Council (Grant No. 621-2010-3971) is greatly appreciated. The authors are grateful to S. L. Chen for his help with PL measurements.

[1]S. J. Pearton, D. P. Norton, K. Ip, Y. W. Heo, and T. Steiner, Prog. Mater. Sci. **50**, 293 (2005).
[2]C. W. Litton, D. C. Reynolds, and T. C. Collins, *Zinc Oxide Materials for Electronic and Optoelectronic Device Applications* (John Wiley & Sons, 2011).
[3]C. Klingshirn, Physica Status Solidi B **244**, 3027 (2007).
[4]T. Dietl, H. Ohno, F. Matsukura, J. Cibert, and D. Ferrand, Science **287**, 1019 (2000).
[5]U. V. Desnica, Prog. Cryst. Growth Charact. Mater. **36**, 291 (1998).
[6]C. G. Van de Walle, D. B. Laks, G. F. Neumark, and S. T. Pantelides, Phys. Rev. B **47**, 9425 (1993).
[7]A. Kobayashi, O. F. Sankey, and J. D. Dow, Phys. Rev. B **28**, 946 (1983).
[8]D. C. Look, D. C. Reynolds, C. W. Litton, R. L. Jones, D. B. Eason, and G. Cantwell, Appl. Phys. Lett. **81**, 1830 (2002).
[9]A. Zeuner, H. Alves, D. M. Hofmann, B. K. Meyer, A. Hoffmann, U. Haboeck, M. Strassburg, and M. Dworzak, Physica Status Solidi B **234**, R7 (2002).
[10]A. Tsukazaki, A. Ohtomo, T. Onuma, M. Ohtani, T. Makino, M. Sumiya, K. Ohtani, S. F. Chichibu, S. Fuke, Y. Segawa, H. Ohno, H. Koinuma, and M. Kawasaki, Nat. Mater. **4**, 42 (2005).
[11]T. M. Barnes, K. Olson, and C. A. Wolden, Appl. Phys. Lett. **86**, 112112 (2005).
[12]J. W. Sun, Y. M. Lu, Y. C. Liu, D. Z. Shen, Z. Z. Zhang, B. Yao, B. H. Li, J. Y. Zhang, D. X. Zhao, and X. W. Fan, J. Appl. Phys. **102**, 043522 (2007).
[13]B. K. Meyer, J. Sann, D. M. Hofmann, C. Neumann, and A. Zeuner, Semicond. Sci. Technol. **20**, S62 (2005).
[14]F. Reuss, C. Kirchner, T. Gruber, R. Kling, S. Maschek, W. Limmer, A. Waag, and P. Ziemann, J. Appl. Phys. **95**, 3385 (2004).
[15]L. Wang and N. C. Giles, Appl. Phys. Lett. **84**, 3049 (2004).
[16]S. Lautenschlaeger, S. Eisermann, B. K. Meyer, G. Callison, M. R. Wagner, and A. Hoffmann, Phys. Status Solidi (RRL) **3**, 16 (2009).
[17]J. Li, S.-H. Wei, S.-S. Li, and J.-B. Xia, Phys. Rev. B **74**, 081201 (2006).
[18]S. Lany and A. Zunger, Phys. Rev. B **81**, 205209 (2010).
[19]J. L. Lyons, A. Janotti, and C. G. V. d. Walle, Appl. Phys. Lett. **95**, 252105 (2009).
[20]J. E. Stehr, D. M. Hofmann, and B. K. Meyer, J. Appl. Phys. **112**, 103511 (2012).
[21]T. Yamamoto and H. Katayama-Yoshida, Jpn. J. Appl. Phys. **38**, L166 (1999).
[22]S. Lautenschlaeger, M. Hofmann, S. Eisermann, G. Haas, M. Pinnisch, A. Laufer, and B. K. Meyer, Physica Status Solidi B **248**, 1217 (2011).
[23]E.-C. Lee, Y. S. Kim, Y. G. Jin, and K. J. Chang, Phys. Rev. B **64**, 085120 (2001).
[24]A. Janotti and C. G. V. d. Walle, Rep. Prog. Phys. **72**, 126501 (2009).
[25]J. E. Stehr, B. K. Meyer, and D. M. Hofmann, Appl. Magn. Reson. **39**, 137 (2010).
[26]G. N. Aliev, S. J. Bingham, D. Wolverson, J. J. Davies, H. Makino, H. J. Ko, and T. Yao, Phys. Rev. B **70**, 115206 (2004).
[27]X. J. Wang, I. A. Buyanova, W. M. Chen, C. J. Pan, and C. W. Tu, J. Appl. Phys. **103**, 023712 (2008).
[28]X. J. Wang, W. M. Chen, F. Ren, S. Pearton, and I. A. Buyanova, J. Appl. Phys. **111**, 043520 (2012).

[29]A. Kaschner, U. Haboeck, M. Strassburg, M. Strassburg, G. Kaczmarczyk, A. Hoffmann, C. Thomsen, A. Zeuner, H. R. Alves, D. M. Hofmann, and B. K. Meyer, Appl. Phys. Lett. **80**, 1909 (2002).
[30]L. Artus, R. Cusco, E. Alarcon-Llado, G. Gonzalez-Diaz, I. Martil, J. Jimenez, B. Wang, and M. Callahan, Appl. Phys. Lett. **90**, 181911 (2007).
[31]F. Friedrich, M. A. Gluba, and N. H. Nickel, Appl. Phys. Lett. **95**, 141903 (2009).
[32]J. B. Wang, H. M. Zhong, Z. F. Li, and W. Lu, Appl. Phys. Lett. **88**, 101913 (2006).
[33]B. K. Meyer, H. Alves, D. M. Hofmann, W. Kriegseis, D. Forster, F. Bertram, J. Christen, A. Hoffmann, M. Straßburg, M. Dworzak, U. Haboeck, and A. V. Rodina, Physica Status Solidi B **241**, 231 (2004).
[34]M. R. Wagner, G. Callsen, J. S. Reparaz, J. H. Schulze, R. Kirste, M. Cobet, I. A. Ostapenko, S. Rodt, C. Nenstiel, M. Kaiser, A. Hoffmann, A. V. Rodina, M. R. Phillips, S. Lautenschläger, S. Eisermann, and B. K. Meyer, Phys. Rev. B **84**, 035313 (2011).
[35]Y. M. Strzhemechny, H. L. Mosbacker, D. C. Look, D. C. Reynolds, C. W. Litton, N. Y. Garces, N. C. Giles, L. E. Halliburton, S. Niki, and L. J. Brillson, Appl. Phys. Lett. **84**, 2545 (2004).
[36]J. Sann, A. Hofstaetter, D. Pfisterer, J. Stehr, and B. K. Meyer, Physica Status Solidi C **3**, 952 (2006).
[37]W. Lim, D. P. Norton, S. J. Pearton, X. J. Wang, W. M. Chen, I. A. Buyanova, A. Osinsky, J. W. Dong, B. Hertog, A. V. Thompson, W. V. Schoenfeld, Y. L. Wang, and F. Ren, Appl. Phys. Lett. **92**, 032103 (2008).
[38]S. J. Jokela and M. D. McCluskey, J. Appl. Phys. **107**, 113536 (2010).
[39]S. J. Jokela and M. D. McCluskey, Phys. Rev. B **76**, 193201 (2007).
[40]J. Kennedy, D. A. Carder, A. Markwitz, and R. J. Reeves, J. Appl. Phys. **107**, 103518 (2010).
[41]X. D. Yang, Z. Y. Xu, Z. Sun, B. Q. Sun, L. Ding, F. Z. Wang, and Z. Z. Ye, J. Appl. Phys. **99**, 046101 (2006).
[42]M. Schirra, R. Schneider, A. Reiser, G. M. Prinz, M. Feneberg, J. Biskupek, U. Kaiser, C. E. Krill, R. Sauer, and K. Thonke, Phys. B: Condens. Matter **401–402**, 362 (2007).
[43]Y. R. Ryu, T. S. Lee, and H. W. White, Appl. Phys. Lett. **83**, 87 (2003).
[44]S. Lautenschlaeger, S. Eisermann, G. Haas, E. A. Zolnowski, M. N. Hofmann, A. Laufer, M. Pinnisch, B. K. Meyer, M. R. Wagner, J. S. Reparaz, G. Callsen, A. Hoffmann, A. Chernikov, S. Chatterjee, V. Bornwasser, and M. Koch, Phys. Rev. B **85**, 235204 (2012).
[45]Z. Q. Chen, A. Kawasuso, Y. Xu, H. Naramoto, X. L. Yuan, T. Sekiguchi, R. Suzuki, and T. Ohdaira, J. Appl. Phys. **97**, 013528 (2005).
[46]S. Stoll and A. Schweiger, J. Magn. Reson. **178**, 42 (2006).
[47]L. S. Vlasenko and G. D. Watkins, Phys. Rev. B **72**, 035203 (2005).
[48]X. J. Wang, L. S. Vlasenko, S. J. Pearton, W. M. Chen, and I. A. Buyanova, J. Phys. D: Appl. Phys. **42**, 175411 (2009).
[49]P. Li, S. Deng, G. Liu, and K. Hou, Chem. Phys. Lett. **543**, 92 (2012).
[50]N. Y. Garces, N. C. Giles, L. E. Halliburton, G. Cantwell, D. B. Eason, D. C. Reynolds, and D. C. Look, Appl. Phys. Lett. **80**, 1334 (2002).
[51]L. S. Vlasenko and G. D. Watkins, Phys. Rev. B **71**, 125210 (2005).
[52]D. Galland and A. Herve, Phys. Lett. A **33**, 1 (1970).
[53]V. A. Nikitenko, J. Appl. Spectrosc. **57**, 783 (1992).
[54]M. C. Tarun, M. Z. Iqbal, and M. D. McCluskey, AIP Adv. **1**, 022105 (2011).